The Periplasmic Domains of *Escherichia coli* HflKC Oligomerize through Right-Handed Coiled-Coil Interactions†

Lee-Ann K. Briere and Stanley D. Dunn*

Department of Biochemistry, University of Western Ontario, London, Ontario N6A 5C1, Canada

Received April 11, 2006; Revised Manuscript Received May 17, 2006

ABSTRACT: The periplasmic domains of the *Escherichia coli* HflK and HflC were coexpressed and purified. The two polypeptides copurified in a 1:1 ratio, as determined by quantitative amino acid analysis. Circular dichroism studies showed the complex to have substantial helical/coiled-coil content that melted with midpoints in the range of 26−29 °C depending upon the concentration, implying a reversible oligomerization. The average molecular weight of the soluble HflKC determined by sedimentation equilibrium ultracentrifugation using a single-species model varied with rotor speed, providing further evidence of concentration-dependent oligomerization. The data were well-fit by models that specified a protomer to *n*-mer oligomerization, with the heterodimeric HflKC as the protomer and values of *n* between 7 and 10. Multiple-sequence alignments of both HflK and HflC revealed regions near the C termini to contain 11-residue hendecad repeats, indicative of right-handed coiled coils, with characteristic small residues in the *a*, *f*, *h*, and *j* positions. To test the importance of the small size of these positions, two residues in the HflC domain, Ala-262 in a *f* position and Gly-268 in an *a* position, were mutated to isoleucine. The HflKC:A262I mutant complex showed lower helicity than the wild type, and its melting was less concentration-dependent. During purification of HflKC:G268I, the mutated HflC subunit precipitated, leaving a preparation of the pure peripheral HflK domain. This polypeptide behaved as a monomer in sedimentation equilibrium experiments and showed low helicity, implying that the protein conformation is largely dependent upon heteromeric subunit interactions. These results demonstrate the importance of right-handed coiled-coil interactions in the oligomerization of HflKC, and a model entailing the formation of a right-handed helical barrel is proposed.

The HflK and HflC polypeptides form a multisubunit complex that is bound to bacterial cytoplasmic membranes through single-membrane-spanning domains located near the N termini of each polypeptide (*1*−*3*). The large, peripheral C-terminal domains composed of residues 101−419 of HflK and 25−334 of HflC in *Escherichia coli* are located in the periplasmic space (*4*). The *hfl* genes were originally identified as loci where the mutation led to a high frequency of lysogenization by phage λ (*5*). It is now known that this effect occurs through their modulation of the activity of the membrane-bound AAA protease FtsH, which degrades the λ cII repressor in addition to a number of *E. coli* membrane proteins (*4*, *6*, *7*). However, the mechanism of this regulation and the overall function of the HflKC complex remain obscure.

On the basis of sequence comparisons, HflKC belongs to the PID (proliferation, ions, and death) or PHB (prohibitin homology) protein superfamily that includes the mitochondrial prohibitin complex, stomatins (band 7), flotillins, and the hypersensitive-induced reaction (HIR)[1] plant disease response genes (*8*−*10*). A range of functions is attributed to these proteins, including action as chaperones (*11*), regulators of membrane channels (*12*), and lipid recognition (*10*), as well as protease modulation.

Little is known about the structure of any members of the superfamily. HflK and HflC are required for the stability of each other in vivo (*13*), and an HflKC complex has been purified following detergent solubilization from membranes, confirming their physical interaction (*6*). The mass of this complex and the number of subunits that it contains have yet to be determined. Recent work shows that a portion of the bacterial complement of HflKC is associated with FtsH in a supercomplex having a sedimentation coefficient higher than 30S, implying a large structure indeed (*14*). The best estimates of the molecular weight of yeast prohibitin are in the range of 1.0−1.2 MDa, although again there is evidence that larger complexes containing other proteins can be formed (*15*, *16*).

† This work was supported by Operating Grant MT-10237 from the Canadian Institutes of Health Research. The Biomolecular Interactions and Conformations Facility is supported by a Multi-User Mainentance and Equipment Grant from the Canadian Institutes of Health Research. Instrumentation in the Drimmer Family Cell Signalling Laboratory was acquired with funds from the Canada Foundation for Innovation. The University of Western Ontario Biological Mass Spectrometry Laboratory is supported by a grant from the Ontario Research and Development Fund.

* To whom correspondence should be addressed. Telephone: 519-661-3055. Fax: 519-661-3175. E-mail: sdunn@uwo.ca.

[1] Abbreviations: A262I complex, complex containing the peripheral domain of wild-type HflK in association with the peripheral domain of HflC carrying the A262I mutation; CD, circular dichroism; HIR, hypersensitive-induced reaction; Phb1 and Phb2, subunits of mitochondrial prohibitin; PID, proliferation, ions, and death superfamily; SDS−PAGE, sodium dodecyl sulfate−polyacrylamide gel electrophoresis.

10.1021/bi0606997 CCC: $33.50
Published on Web 06/21/2006

To learn more about the interactions and structure of HflKC, we coexpressed the periplasmic domains of the two polypeptides in the absence of the N-terminal membrane domains and studied them using the biophysical techniques of circular dichroism (CD) spectropolarimetry and analytical ultracentrifugation. Here, we show that the soluble domains assemble reversibly into oligomers and that they contain significant helical character. Furthermore, we have identified sequences near their C termini that contain an unusual 11-residue repeat motif indicative of right-handed coiled coils, and we present mutational evidence of the importance of these sequences for oligomerization.

EXPERIMENTAL PROCEDURES

Plasmid Construction. Recombinant DNA techniques were carried out using standard procedures. Polymerase chain reactions were performed using Taq polymerase (Fermentas) and a touch-down protocol. Plasmid pKH178 (*6*) or derivatives were used as templates. All constructs were verified by DNA sequencing and restriction enzyme mapping.

Plasmid pLB8 was designed to coexpress the periplasmic domains of HflK and HflC. The sequence encoding residues Lys101−Glu419 of HflK was amplified using oligonucleotides with sequences of CAGCTGGCGCCGAAGCCGAACGC and CAGCTGGATCCCATCGTTATTCCCCCT as forward and reverse primers, respectively. The sequence encoding Gly25−Arg334 of HflC was amplified using oligonucleotides CAGCTGGATCCGAAGGTGAGCGC and CAGCTAAGCTTTTAACGCGTTGCG as forward and reverse primers, respectively. *Ehe*I, *Bam*HI, and *Hin*dIII restriction sites used during the assembly of the product to produce the soluble HflKC construct are underlined. The products were combined using the *Bam*HI sites, cleaved with *Ehe*I and *Hin*dIII, and inserted into pJB3 (*17*), which had been digested with *Sca*I and *Hin*dIII, to produce pLB8. The HflK sequence is preceded by codons for methionine and serine; the HflC sequence is preceded by codons for methionine, glycine, and serine.

Plasmid pLB9 was identical to pLB8 except for a mutation encoding a G268I change in HflC. The HflC sequence was amplified by the mutagenic primer CAGCTGCTGAGCGTCAG**ATT**CGCATCATGCGTGG and the reverse HflC primer above. The *Blp*I site used for cloning is underlined, and the mutagenic codon is shown in bold. The product was inserted into pLB8 using the *Blp*I and *Hin*dIII sites. Plasmid pLB10 was identical to pLB8, except for a mutation encoding an A262I change in the HflC subunit. The DNA was amplified by the mutagenic primer CAACTGCTCAGCTTC**AAT**CAGCGTTCTGGTCAC and the forward HflC primer from the construction of pLB8. The *Blp*I site used for cloning is underlined, and the mutagenic codon is shown in bold. The product was inserted into pLB8 using the *Blp*I and *Bam*HI sites.

Expression and Purification of Soluble HflKC. Peripheral domains of HflK and HflC were expressed from pLB8 in *E. coli* strain MM294 (*18*), grown in 1 L cultures of 2× YT medium (Becton Dickinson) containing 40 μg/mL ampicillin. Initial cell growth was at 37 °C. When A_{600} reached a value of 0.5−0.8, expression was induced by the addition of 0.3 mM isopropylthiogalactoside and the temperature was reduced to 30 °C. A total of 3−6 h later, the cells were harvested by centrifugation and stored frozen at −80 °C.

Purification of the soluble domains of HflK and HflC was carried out at 4 °C and was followed by sodium dodecyl sulfate−polyacrylamide gel electrophoresis (SDS−PAGE) using the buffer system of Laemmli (*19*). Cells from 1 L of culture were suspended in 50 mM Tris-HCl and 10 mM $MgCl_2$ at pH 8.0 to produce a 10% cell suspension. Phenylmethanesulfonyl fluoride and *p*-aminobenzamidine-HCl were added to concentrations of 1 and 5 mM, respectively, and then the cells were disrupted by one passage through a French pressure cell at 20 000 psi. The peripheral domains of HflK and HflC were sedimented by centrifugation for 10 min at 10 000 rpm in a Beckman JA-20 rotor. The precipitates were washed by resuspension in 50 mM Tris-HCl and 10 mM $MgCl_2$ at pH 8.0 and subsequent centrifugation, and then the step was repeated using 1 M NaCl, 50 mM Tris-HCl, and 1 mM ethylenediaminetetraacetic acid (EDTA) at pH 8.0. HflK and HflC were solubilized by homogenizing the pellet in 1 M guanidine-HCl, 100 mM Tris-HCl, and 1 mM EDTA at pH 8.0 and stirring on ice for 1 h. After centrifugation to remove insoluble material, the supernatant solution was dialyzed into 50 mM Tris-HCl, 10% glycerol, and 1 mM EDTA at pH 8.0 (TGE buffer) and then loaded onto a DEAE-Sepharose column (30 × 1.5 cm), and proteins were eluted with a linear gradient of 0−300 mM NaCl in TGE buffer. Fractions containing HflKC were pooled, dialyzed into TGE buffer, and loaded onto a hydroxyapatite column (5 mL bed volume). HflKC was eluted with a linear 0−300 mM gradient of sodium phosphate at pH 8.0 in TGE buffer. Pure protein samples were frozen and stored at −80 °C. After thawing, samples were centrifuged for 3 h at 38 000 rpm to remove insoluble material that formed during storage and thawing, before all subsequent structural analyses. Soluble HflKC:A262I was purified using the same procedure. HflC:G268I precipitated during purification of the HflKC:G268I complex, and pure preparations of HflK were eluted from the hydroxyapatite column.

Amino Acid Analysis and Mass Spectrometric Identification of Proteins. Quantitative amino acid analysis of samples was carried out in triplicate at the Alberta Peptide Institute (University of Alberta, Edmonton, Canada). The yields of Ala, Arg, Asx, Glx, and Lys were used in conjunction with the inferred amino acid composition to calculate the total protein concentrations. Correction factors for protein assays using the Coomassie Blue (BioRad) and Advanced (Cytoskeleton) reagents, using bovine serum albumin as the standard, were determined.

Protein bands were robotically excised from polyacrylamide gels and digested with trypsin in the Drimmer Family Cell Signalling Laboratory at the University of Western Ontario. Mass spectrometric analysis of peptides was done using a Micromass matrix-assisted laser desorption ionization (MALDI)-R mass spectrometer in the Dr. Don Rix Protein Identification Facility in the University of Western Ontario Biological Mass Spectrometry Laboratory. Data were analyzed using ProteinLynx software. The slower migrating band of the HflKC peripheral domain complex was identified as the HflK component, with 52% coverage of the wild-type amino acid sequence compared to a possible 78% coverage. The faster migrating band was identified as the HflC component, with 43% coverage compared to a possible 93% coverage of the wild-type amino acid sequence.

CD Spectroscopy. CD studies were performed on a Jasco J-810 spectropolarimeter equipped with a Peltier temperature control system (Biomolecular Interactions and Conformations Facility, University of Western Ontario). A cell with a path length of 0.1 cm was used. Protein samples were dialyzed into buffer containing 10 mM sodium phosphate at pH 7.5, 10% glycerol, and 1 mM EDTA. CD spectra were collected at 5 °C in 0.5 or 1 nm steps at scan speeds of 5−20 nm/min. CD values were converted to mean residue ellipticity (θ) in units of degree cm^2 dmol^{-1} by standard procedures.

Protein denaturation was followed in the CD at 222 nm. The temperature was increased at a rate of 1 °C/min. Inflection points from the melting curves were determined using a linear extrapolation method (*20*, *21*) and by fitting to eq 1 using Prism 4 software (GraphPad) as described (*22*).

$$y = \frac{(y_n + m_n x) + (y_d + m_d x)\exp\left[\frac{\Delta H_m}{R}\left(\frac{1}{T_m} - \frac{1}{x}\right)\right]}{1 + \exp\left[\frac{\Delta H_m}{R}\left(\frac{1}{T_m} - \frac{1}{x}\right)\right]} \quad (1)$$

In this expression, x is the temperature in Kelvin, y_n and y_d refer to the y intercepts of the native and denatured baselines, respectively, m_n and m_d are the slopes of the baselines, R is the gas constant in kcal mol^{-1} K^{-1}, T_m is the temperature at the midpoint of the transition, and ΔH_m is the enthalpy of unfolding at T_m in kcal/mol. In the absence of a specific model for unfolding of HflKC, the fitted ΔH_m values lack quantitative thermodynamic significance and were used here as a semiquantitative indicator of the cooperativity of unfolding.

Analytical Ultracentrifugation. Sedimentation equilibrium studies were carried out using a Beckman Optima XL-A Analytical Ultracentrifuge (Biomolecular Interactions and Conformations Facility, University of Western Ontario). An An60Ti rotor and six-channel cells with Epon-charcoal centerpieces were used. Protein samples were dialyzed into 10 mM sodium phosphate, 10% glycerol, 1 mM EDTA, and 100 mM NaCl at pH 7.5 buffer and diluted to the desired concentration. Centrifugation was carried out at 5 °C. Absorbance measurements at 280 or 230 nm were collected in 0.002 cm radial steps and averaged over 10 readings. The densities of solvents were calculated from published tables. Partial specific volumes of both soluble HflKC and soluble HflK were calculated from their amino acid compositions (*23*) to be 0.73 mL/g.

Data were analyzed using models constructed in Prism 4 (Graphpad). A single ideal species model was defined by eq 2.

$$c_r = c_o \exp\left[\frac{\omega^2}{2RT} M_{obs}(1 - \bar{v}\rho)(r^2 - r_o^2)\right] + I_o \quad (2)$$

where c_r is the concentration at radius r, c_o is the concentration at reference radius r_o, ω is the angular velocity of the rotor, M_{obs} is the molecular weight of the protein, $\bar{v}$ is the partial specific volume of the protein, ρ is the density of the solvent, R is the ideal gas constant, T is the temperature in Kelvin, and I_o is the baseline offset. A series of protomer:n-mer models with different values of n were also constructed; equilibrium constants, K_A, for such models are defined by eq 3.

$$K_A = \frac{[n\text{-mer}]}{[\text{protomer}]^n} \quad (3)$$

Sedimentation equilibrium data for HflKC were subsequently fit to the protomer:n-mer models using eq 4.

$$c_r = \left\{c_o \exp\left[\frac{\omega^2}{2RT} M_p(1 - \bar{v}\rho)(r^2 - r_o^2)\right]\right\} + \left\{c_o{}^n K_A \exp\left[\frac{\omega^2}{2RT} n M_p(1 - \bar{v}\rho)(r^2 - r_o^2)\right]\right\} + I_o \quad (4)$$

In this expression, M_p is the mass of the protomer and other terms are as defined above. Fits were tested using a runs test in Prism 4 (Graphpad).

RESULTS

Multiple-Sequence Alignments of HflK and HflC Reveal an 11-Residue Repeat Pattern. Visual inspection of alignments of HflK and HflC sequences from a range of bacterial classes (parts A and B of Figure 1) reveal the C-terminal domains of each to contain unusual 11-residue hendecad repeats, (*abcdefghijk*)$_n$, with small residues in the *a*, *h*, and *j* positions and larger, hydrophobic residues often in the *d* and *e* positions. The hendecad region of HflC also has small residues in the *f* positions. To determine if the hendecad pattern identified represents the major periodicity of this region, sequence alignments were analyzed by Fourier transform using the FTwin program of the online REPPER server (*24*). REPPER can analyze individual sequences, user-supplied sequence alignments, or PSI-BLAST alignments generated by the server, using either standard criteria provided in the program or values assigned by the user. Some of the expected periodicities that might be seen with an undecad pattern, i.e., 11, 11/2, 11/3, 11/4, and 11/5, were evident when either the standard binary or Kyte−Doolittle hydropathy criteria provided by the server were applied to the sequence alignments (data not shown). However, because the pattern is based on both size and hydrophobicity, it is not surprising that the clearest results were obtained using criteria designed to distinguish between the types of residues that we have observed in the different positions. Glycine and alanine were given large positive values; serine, threonine, and valine, which sometimes occur in positions dominated by alanine, were given smaller positive values; large hydrophobic residues were given large negative values; and polar residues, proline and cysteine, were given null value, as described in the caption of Figure 1. Results obtained by applying these criteria to the hendecad regions of HflK and HflC PSI-BLAST profiles are shown in parts C and D of Figure 1. For HflK, the three strongest periodicities correspond to 11/5, 11, and 11/2, while for HflC, the pattern is even stronger, as ratios of 11 constitute the five strongest peaks. Similar but slightly less precise periodicities were obtained using only the sequences aligned in parts A and B of Figure 1 (data not shown). These analyses provide strong objective support for the generality of the hendecad pattern identified in the sequences shown.

Hendecad patterns are indicative of an unusual type of coiled coil in which 11 residues make 3 helical turns with

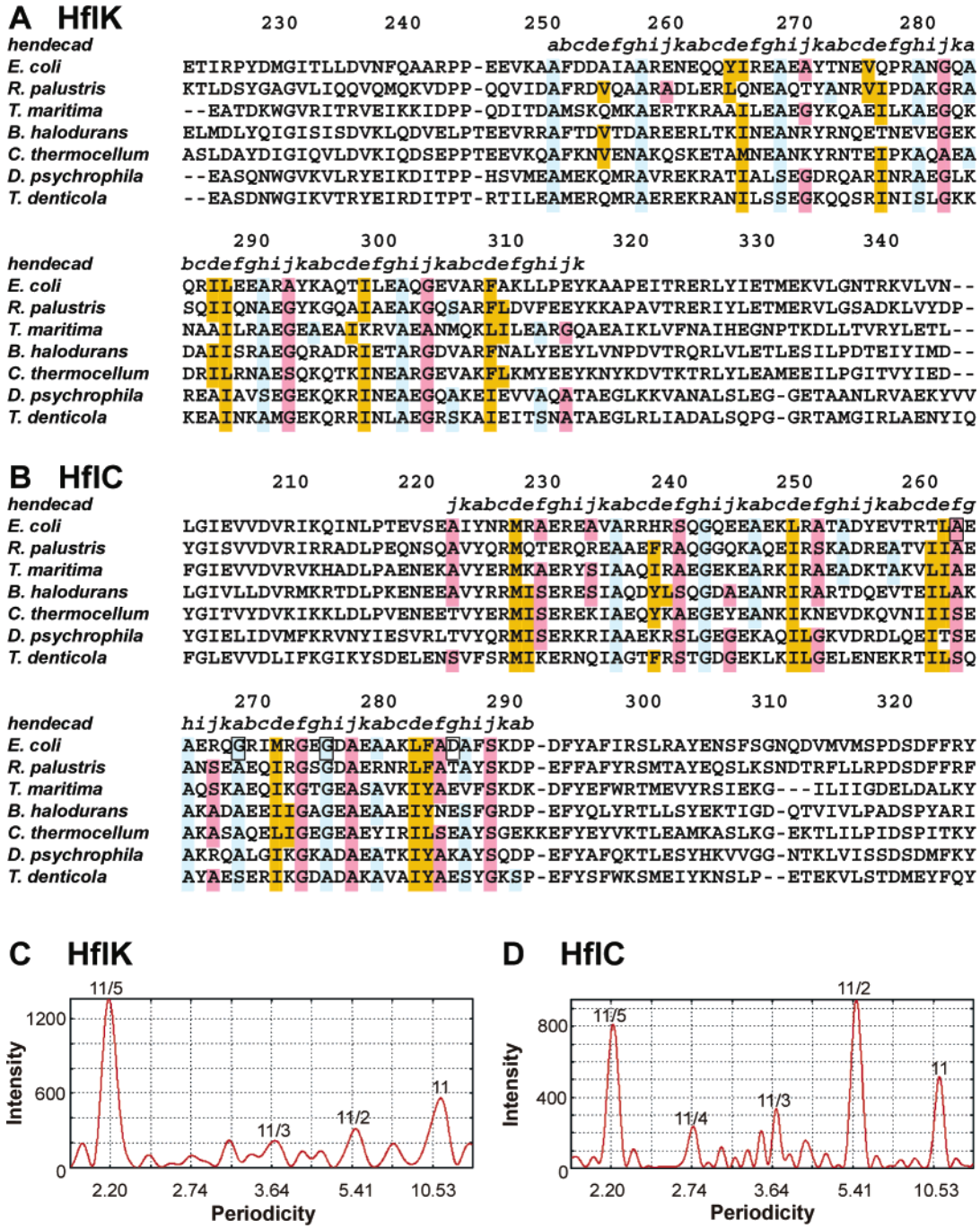

FIGURE 1: Sequence alignments of the coiled-coil regions of HflK (A) and HflC (B) sequences from seven phylogenetically distinct bacteria. Sequences used in the alignment were from the following species (phylogenetic taxon): *E. coli* (*Gammaproteobacteria*), *Rhodopseudomonas palustris* (*Alphaproteobacteria*), *Thermotoga maritima* (*Thermotogae*), *Bacillus halodurans* (*Bacilli*), *Clostridium thermocellum* (*Clostridia*), *Desulfotalea psychrophila* (*Deltaproteobacteria*), and *Treponema denticola* (*Spirochaetes*). Each set of sequences was submitted to the online multiple-sequence alignment program ClustalW (EMBL-EBI, European Bioinformatics Institute). The default parameters were used. The upper line shows the hendecad positions. For both alignments, small residues (AGS) in the *a* or *h* positions are highlighted in blue, while larger hydrophobic residues (FILMVY) in the *d* or *e* positions are highlighted in gold. Small residues (AGS) in the *f* positions of HflK or in the *f* or *j* positions of HflC are highlighted in pink. In the *E. coli* HflC sequences, positions Ala-262 and Gly-268, mutated in this study and positions Gly-275 and Asp-285 that are altered in the *hfl-1* mutant (*5*) are shown in boxes. The periodicities of the amino acid sequences of positions 265−315 of HflK (C) and 223−295 of HflC (D) were analyzed using the FTwin component of REPPER [Max Planck Institute for Developmental Biology, Tübingen, Germany (*24*)]. Profiles were calculated by PSI-BLAST using the *E. coli* sequences as input. Amino acid residues were assigned the following values: A and G, 5; S, 3; V and T, 1; C, D, E, H, K, N, P, Q, and R, 0; F, I, L, M, W, and Y, −5.

respect to the core, forming a right-handed coiled coil with a hydrophobic periodicity of 3.67 (11/3), just as heptad patterns are indicative of left-handed coiled coils in which 7 residues make 2 turns, forming a left-handed coiled coil with a hydrophobic periodicity of 3.5 (7/2) (*25*−*27*). Similar to the *a* and *d* positions of the heptad in left-handed coiled coils, by convention, the *a*, *d*, *e*, and *h* positions of the hendecad are located on the side of the helix involved in interhelical interactions and are typically occupied by hydrophobic residues, as seen in the high-resolution structure

of the four-stranded right-handed helical bundle of a bacterial surface tetrabrachion (*28*). While no parallel, two-stranded right-handed coiled coil has yet been defined at high resolution, small residues in the *a* and *h* hendecad positions were suggested to be essential to such a structure, because larger side chains in these positions would cause steric clashes (*25*). The residue pattern seen in HflK and HflC thus suggests that these polypeptides interact along the surfaces containing the *a*, *d*, *e*, and *h* positions to form heterodimeric right-handed coiled-coil interactions. The small residues in the *j* and *f* positions, located on the side of each helix opposite the *adeh* surface (see Figure 5), could provide surfaces for higher order oligomerization of HflKC dimers through additional right-handed coiled-coil interactions. To investigate these possibilities, we undertook the structural characterization of HflKC.

Expression and Purification of Soluble HflKC. Initially, the complete HflKC complex was purified by a published technique (*6*), but despite the use of protease-deficient strains, the product became degraded too rapidly for transfer into UV-transparent detergents and structural characterization (data not shown). Soluble forms of HflK (residues 101−419) and HflC (residues 25−334) lacking the N-terminal membrane domains were therefore prepared to allow for structural characterization of the periplasmic domains containing the hendecad repeats. In the *E. coli* chromosome, *HflK* and *HflC* are adjacent cistrons linked by the sequence GGGGAATAACGATGCGT, where the *HflK* stop codon and *HflC* start codon are underlined. Given the proximity of these signals and the apparent Shine−Dalgarno sequence just before the *HflK* stop codon, this arrangement likely provides for stoichiometric expression of the two polypeptides through ribosomal reinitiation. A similar relationship was engineered in plasmid pLB8, but the downstream *HflC* start codon was followed by an in-frame *Bam*HI site used in cloning, then by the codons for residue Glu-25, and the rest of *HflC*. The inferred molecular weights of the peripheral domains of HflK and HflC, as expressed, were 35 527 and 35 209, respectively. As seen in the SDS extract of induced cells shown in Figure 2A, the two polypeptides were resolved by SDS−PAGE, revealing an expression ratio of approximately 1:1. The identities of the two polypeptides were confirmed by mass spectrometric analysis of tryptic digests as described in the Experimental Procedures (data not shown).

After cell lysis, the polypeptides, which initially sedimented at low speed, could be solubilized using just 1 M GuHCl and remained in solution during dialysis against buffer containing glycerol. The soluble HflK and HflC polypeptides were then purified by ion-exchange and hydroxyapatite column chromatography. HflK and HflC repeatedly coeluted in an apparent 1:1 ratio (Figure 2B), suggesting their heteromeric association. This stoichiometry was confirmed through quantitative amino acid analysis undertaken to determine exact protein concentrations for CD studies (Table 1). Residues used in this analysis (Ala, Arg, Asx, Glx, and Lys) were selected on the basis of their efficient recovery following hydrolysis and, in the case of Glx residues, also because of a large difference in composition within HflK and HflC subunits. Data are presented as the mol % of this group of residues only. The best fit of polypeptide stoichiometry to the data, determined by the minimum sum of squares method, was 1.023 mol of HflK/1 mol of HflC. Experimental data were in excellent agreement with a 1:1 ratio; the expected results for 2:1 and 1:2 molar ratios are shown for a comparison. This result is most consistent with the assignment of an HflKC heterodimer as the protomer for oligomer formation.

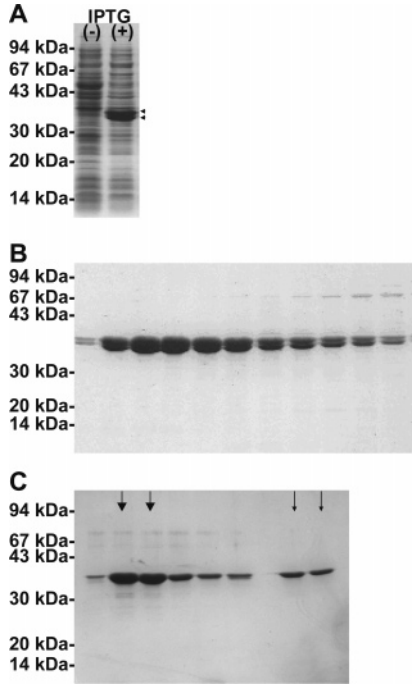

FIGURE 2: Expression and purification of the soluble domains of HflK and HflC. (A) *E. coli* strain MM294 containing pLB8 was grown either with or without induction by 0.3 mM isopropylthiogalactoside. Proteins were extracted from cells with SDS sample buffer and analyzed by SDS−PAGE. The induced polypeptides may be seen as the closely spaced pair of bands migrating with apparent molecular weights of 34 000−35 000. (B) Coelution of the HflK and HflC polypeptides from DEAE-Sepharose during purification of the complex. Successive column fractions containing the protein peak were analyzed by SDS−PAGE. (C) Elution of pure HflK from the hydroxyapatite column. The standard purification procedure was applied to HflKC:G268I. Successive column fractions containing the protein peak of HflK were analyzed by SDS−PAGE. The two lanes to the right received smaller samples of the fractions indicated by the arrows, to confirm that single bands were present.

Table 1: Determination of HflKC Peripheral Domain Ratio from Amino Acid Composition

residue	number in K	number in C	observed mol % ± SD[b]	expected mol %[a]		
				K_2C_1	K_1C_1	K_1C_2
Ala	34	32	21.43 ± 0.04	21.46	21.36	21.26
Arg	27	31	18.80 ± 0.06	18.24	18.77	19.31
Asx	35	36	22.80 ± 0.07	22.75	22.98	23.21
Glx	47	35	26.50 ± 0.10	27.68	26.54	25.38
Lys	14	18	10.48 ± 0.04	9.87	10.36	10.85
sum of squares[c]				2.07	0.05	1.85

[a] The expected mol % of residues listed in this table only, on the basis of inferred amino acid sequences and subunit stoichiometry indicated. [b] The mol % of residues listed in this table only, as determined by quantitative amino acid analysis carried out in triplicate. [c] Sum of the squares of differences between observed and expected mol % for each indicated subunit stoichiometry.

Introduction of Mutations in the Hendecad Repeat. The role of the hendecad repeat in the interaction between HflK and HflC was studied by mutating the small residues in two positions of the HflC subunit to the larger isoleucine,

introducing bulk but not polarity or charge. In one case, HflC Gly-268 in an *a* position was mutated (G268I), while in the other, HflC Ala-262 in a *f* position was changed (A262I). These are two of the positions highlighted by boxes in the *E. coli* HflC sequence (Figure 1). Both protein complexes were overexpressed and purified using the protocol established for the soluble HflKC complex. During the refolding and purification procedure for the G268I mutant, the HflC:G268I subunit precipitated, while HflK remained in solution and was recovered from the hydroxyapatite column in pure form (Figure 2C). The A262I mutant behaved similarly to the wild-type soluble complex, in that HflK and HflC copurified in a 1:1 ratio, judging from the staining intensities. However, the complex was more susceptible to precipitation during the refolding process and had lower solubility once purified, compared to the wild-type protein.

Analysis of Structure and Stability by CD Spectroscopy. CD spectroscopy was used to analyze the secondary structures of the HflK subunit, soluble HflKC, and the HflKC:A262I complex in solution. CD spectra of HflKC and A262I complexes seen in Figure 3A showed prominent minima at 222 and 208 nm, with signal intensities at 222 nm of $-16\,600°$ and $-13\,900°$ cm^2 dmol^{-1} for HflKC and the HflKC:A262I mutant, respectively, indicating the presence of a substantial helical structure. Analysis of the spectra using SELCON 3 (*29*) indicated 40 and 33% helical content for HflKC and the A262I mutant complexes, respectively. In contrast, the isolated HflK had a signal intensity of just $-6800°$ cm^2 dmol^{-1} at 222 nm, indicating that the polypeptide possessed only a low level of helical structure in the absence of HflC. It is also notable that the $\theta_{222}/\theta_{208}$ ratios for HflKC, HflKC:A262I, and HflK were 0.92, 0.94, and 0.76, respectively. Noninteracting helices typically give ratios of around 0.8, while in coiled coils, the ratio is close to 1.0 (*30*); therefore, these spectra imply that many of the helical residues in the complexes are in coiled-coil interactions.

CD was also used to follow the thermal denaturation of HflK, HflKC, and HflKC:A262I by observing changes in the signal at 222 nm as the temperature was increased from 5 to 85 °C (Figure 3B). The pure HflK exhibited only a modest transition at 59 °C. This transition was independent of the concentration, implying that it represented an intramolecular change. Together with the spectrum in Figure 3A, the relatively high temperature of this transition suggests the possibility that HflK retains some residual structure in the absence of HflC. In contrast, the heteromers showed much larger transitions at lower temperatures, while a second higher-temperature transition, presumably because of the HflK in the sample, was just visible in those plots. The effect of the protein concentration on the CD signal and the primary thermal denaturation transition was determined for the heteromeric complexes (Figure 3C). While the CD signal of HflKC was dependent upon the concentration at lower temperatures and concentration-dependent changes were evident in the denaturation curves, the signal of the A262I mutant was largely independent of the concentration. Each denaturation curve was fitted to eq 1 describing a two-state transition as described in the Experimental Procedures to determine the midpoint of the transition, T_m, and to provide a semiquantitative measure of the cooperativity as indicated by the apparent enthalpy of unfolding at the midpoint, ΔH_m.

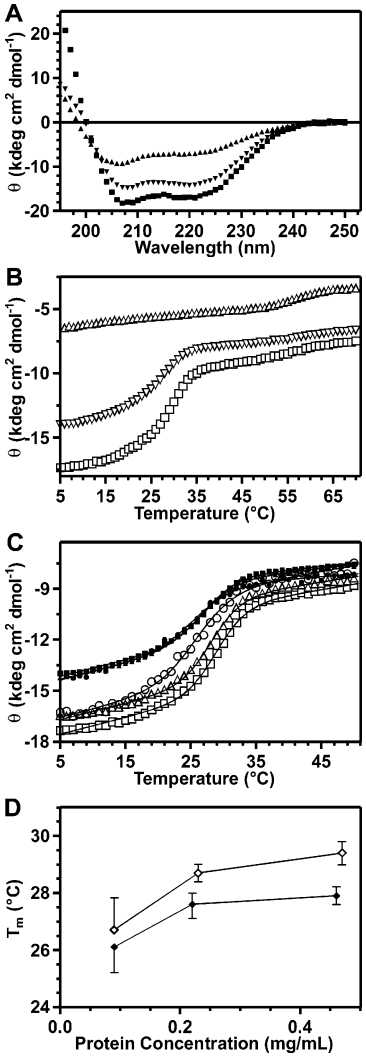

FIGURE 3: Analysis of soluble domains of HflKC by CD. (A) CD spectra of HflKC (■), HflKC:A262I (▼), and isolated HflK (▲), each at a concentration of 0.50 mg/mL, were collected as described under the Experimental Procedures. (B) Thermal denaturation of HflKC (0.47 mg/mL, □), HflKC:A262I (0.46 mg/mL, ▽), and pure HflK (0.35 mg/mL, △) was studied by following the CD signal at 222 nm as the temperature was raised. (C) Effect of the protein concentration on the major thermal transitions of HflKC (0.09 mg/mL, ○; 0.23 mg/mL, △; 0.47 mg/mL, □) and the A262I mutant complex (0.09 mg/mL, ●; 0.22 mg/mL, ▲; 0.46 mg/mL, ■) was determined. Fits of each experimental data set to a two-state transition model are shown by the solid lines. (D) Effect of the protein concentration on T_m for HflKC (◇) and the A262I complex (◆) is shown, as derived from fits to the data in C. Error bars indicate the 95% confidence intervals.

The lines of best fit are drawn in Figure 3C, and the inferred T_m values are presented as a function of the protein concentration in Figure 3D. At the lowest concentration used, 0.09 mg/mL, the melting temperatures of soluble HflKC and the A262I mutant were essentially identical, but as the protein concentration was increased, the T_m for wild-type HflKC increased much more sharply than that for the A262I complex. The cooperativity of unfolding of HflKC, measured by the apparent ΔH_m, also increased more dramatically with the concentration than that of the HflC:A262I mutant (data not shown). It may be noted in Figure 3C that the two-state model provided good fits to the data for lower concentrations but not higher concentrations of HflKC, whereas the model provided reasonable fits at all concentrations of the A262I

Table 2: Molecular Weight of the HflKC Peripheral Complex by Sedimentation Equilibrium

rotor speed (rpm)	observed molecular weight
5000	270 300
8000	194 200
10 000	190 400
15 000	79 800

[a] Sedimentation equilibrium analytical ultracentrifugation was carried out as described under the Experimental Procedures. The initial protein concentration of HflKC was 0.7 mg/mL. The molecular weight that provided the best fit of the data to a single ideal species model is shown.

mutant. Together, these results imply that HflKC existed in more than one oligomeric state and that at higher concentrations the predominant form was more stable and more highly oligomerized than the predominant form at lower concentrations. The less oligomerized form would appear to be at least a heterodimer, because the pure HflK gave only a slight helical signal. The relatively smaller effects of the protein concentration on the spectral and denaturation properties of the A262I mutant form suggest that its ability to undergo the higher order oligomerization is impaired.

Sedimentation Equilibrium Analyses. Oligomerization of the soluble HflK, HflKC, and HflKC:A262I proteins was also studied using sedimentation equilibrium analytical ultracentrifugation. A range of protein concentrations and rotor speeds were used in the studies. Initial analyses of the data were carried out assuming a single ideal species model.

HflK studied at initial concentrations between 0.45 and 0.9 mg/mL and rotor speeds between 15 000 and 30 000 rpm gave good fits for a single species with a molecular weight of 35 000 ± 3100 (average ± standard error of the mean), in good agreement with the expected monomer molecular weight of 35 526.7. In contrast, the average molecular weight calculated for samples of HflKC changed dramatically with the rotor speed (Table 2), and the residuals obtained from these fits were not randomly distributed, again implying a concentration-dependent self-association behavior. Sample data collected at 8000 rpm are shown in Figure 4A; here, the best fit of the molecular weight for a single species was 194 000. The simplest models for association entail the oligomerization of *n* protomers into an *n*-mer complex. Here, we assumed the HflKC heterodimer to be the protomer, with a molecular weight of 70 735 based on the sequences. Models were constructed for values of *n* ranging from 2 to 16, and the data were fit to the appropriate equations as described in the Experimental Procedures. A fit of the data collected at 8000 rpm to the protomer:octamer model, shown in Figure 4B, revealed essentially randomly distributed residuals. Three data sets obtained under differing conditions were fitted to each value of *n*. The goodness of each fit was judged by the resulting *p* value for the runs test, where higher *p* values indicate an increasing likelihood that the residuals are randomly distributed. Plots of *p* values as a function of *n* (Figure 4C) indicate that models specifying the oligomerization of 7−10 protomers provided the best fits. Attempts to conduct sedimentation equilibrium analysis using the HflKC:A262I mutant protein gave unreliable results because of the precipitation of the protein during the extended equilibrium runs. However, in some cases, fits of the data to the single-species model gave molecular weights substantially higher than that of the protomer (data not shown), implying that oligomerization was not completely disrupted by the mutation.

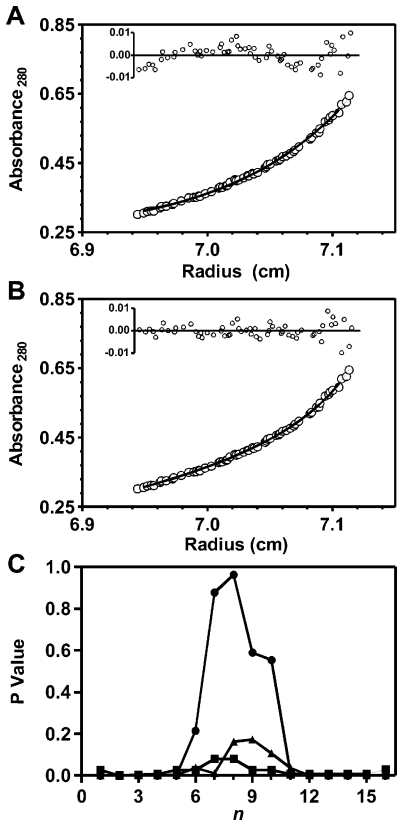

FIGURE 4: Sedimentation equilibrium analysis of the soluble domains of HflKC. (A and B) Sample of HflKC with an initial concentration of 0.7 mg/mL was centrifuged at 5 °C at a rotor speed of 8000 rpm until equilibrium was reached. The cell was scanned at 280 nm. In A, the data were fitted to a single ideal species model, while in B, the same data were fitted to a protomer:octamer model, where the protomer was taken to be an HflKC heterodimer with a molecular weight of 70 735. The insets show the residuals. (C) Analysis of sedimentation equilibrium data fits using the runs test. Sedimentation equilibrium data were collected at 280 nm for samples with an initial concentration of 0.70 mg/mL at rotor speeds of 5000 (■) and 8000 (▲) rpm and at 230 nm for another sample with an initial concentration of 0.065 mg/mL at a rotor speed of 10 000 rpm (●). Each data set was fitted to protomer:*n*-mer models with values of *n* from 2 to 16, and the fits were analyzed by the runs test, with higher *p* values indicating an increased probability that the residuals were distributed randomly.

DISCUSSION

Previous work has shown that the HflK and HflC polypeptides of *E. coli* are mutually dependent for stability in vivo and that the polypeptides associate to form large membrane-bound oligomers. However, little physical analysis of these structures has been carried out, and there has been no information on the importance of the membrane-spanning domains for assembly of the complex. Here, we have shown that, after deleting the N-terminal sequences containing the single membrane-spanning domains of each polypeptide, the resultant soluble domains retained the ability to form a heteromeric complex that exists in equilibrium between a protomer, likely to be the heterodimer, and higher order species. The CD studies confirmed that these proteins are folded and demonstrated that the structure of HflK is dependent upon interactions with HflC. Reversible higher order oligomerization of the heterodimeric protomers was

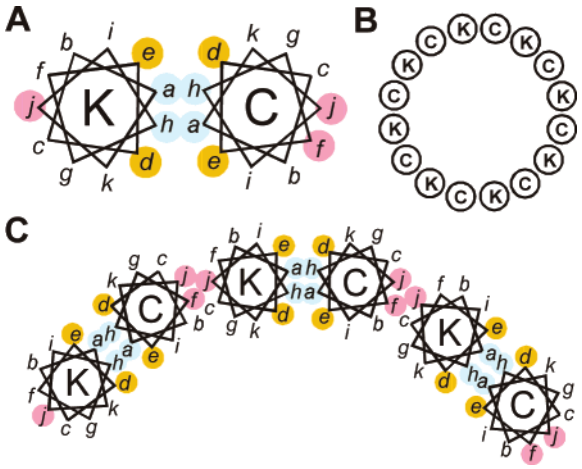

FIGURE 5: Model for the oligomerization of the soluble domains of HflKC. (A) Cross-sectional view of the proposed two-stranded right-handed coiled coil in the HflKC protomer showing the hendecad positions, with positions highlighted as in Figure 1. (B) Proposed arrangement of eight-paired coiled-coil regions of HflK and HflC to form a right-handed barrel containing 16 helices. (C) Helix−helix interactions of HflK and HflC in the barrel. A section of a heterohexadecameric barrel structure made from eight HflKC protomers is shown, although the barrel may contain a different number. The *ahde* faces of each subunit are suggested to interact initially to form the heterodimeric HflKC protomer. Interactions between HflKC protomers to form the closed barrel are proposed to occur between the *fj* faces.

indicated by the concentration-dependent increases in melting temperatures, molecular weights, and cooperativity of denaturation. Good fits to the sedimentation data were obtained for models that specified 7−10 HflKC protomers in the complex.

We suggest that the previously unrecognized 11-residue (hendecad) repeats, indicative of right-handed coiled coils (*27*), located toward the C termini of the peripheral domains, provide interactions critical to oligomerization. Given the helical CD spectra of the protein and the pronounced effects of mutations in the hendecad repeats, it seems likely that oligomerization occurs through right-handed coiled-coil interactions. Because the *a*, *d*, *e*, and *h* positions in the hendecad repeats, which are located on one side of the helix, are occupied by characteristic residues in both the HflK and HflC subunits, we propose that the initial heterodimer interaction occurs through these faces (Figure 5A), producing a two-stranded right-handed coiled coil related to that proposed for the *b* subunit of the F_1F_o-ATP synthase (*31*, *32*). This possibility is supported by the near-complete disruption of polypeptide interactions by the HflC:G268I mutation, which affects an *a* position. The strong preference for small residues at this position implies that the bulky isoleucine would be too large and, in the proposed model, would be expected to weaken heterodimer assembly. During purification, the HflC polypeptide precipitated, while the HflK monomer remained in solution. Steric disruption of the heterodimer interface is the most likely explanation for the properties of this mutant in our view, although other effects such as intrinsic misfolding of the HflC polypeptide caused by the G268I mutation cannot be ruled out. Notably, the original *hfl-1* mutant described in 1971 (*5*) was subsequently shown to carry two mutations causing amino acid changes in HflC, G275D and D285H (*13*), both located in the hendecad region that we have identified. The G275D mutation, which affects an *h* position, would be expected to disrupt the heterodimer interface in our model.

The hendecads of HflK and HflC differ from those previously identified in the F_1F_o-ATP synthase *b* subunit in that small, hydrophobic residues also occur at the *j* positions of HflK and both the *j* and *f* positions of HflC. Because these positions are situated nearly opposite the *a* and *h* positions, they form additional faces that could constitute surfaces for the higher order oligomerization (Figure 5), resulting in the formation of a barrel of helices related by right-handed twists. While the mutation of Ala-262 of HflC, which occupies an *f* position, to isoleucine did not prevent assembly, the reduced helicity and the reduced concentration-dependent changes in T_m and cooperativity of unfolding for this protein are most consistent with altered interactions in a coiled-coil oligomerization interface. Together, the effects of the mutations described here on the physical behavior of the peripheral domains of HflKC, the functional defects in the Hfl-1 mutant previously described (*5*, *13*), and the results of our biophysical studies provide multiple lines of support for the model that we formulated on the basis of the bioinformatic analysis. However, additional mutational testing of the model will be necessary to establish it firmly, and we cannot distinguish with certainty between the arrangement proposed in Figure 5 and one in which the *a*/*h* surface of each subunit interacts with the *f*/*j* surface of the other.

The peripheral domains of HflKC are located in the periplasmic space, and it is interesting to note that the similarly situated TolC protein also forms a helical barrel with a central cavity (*33*). In this case, the barrel is composed of 12 helices, 4 from each of the 3 identical subunits, and these helices interact in the commonly seen left-handed manner. One example of a right-handed helical barrel can be found in the crystal structure of MscS, the heptameric small-conductance mechanosensitive membrane channel of *E. coli* (*34*). Here, each subunit contributes one helix containing residues 96−110 to produce a right-handed heptameric helical barrel. As in the coiled-coil regions that we have identified in HflK and HflC, this part of the MscS sequence is rich in highly conserved small residues, and the crystal structure shows the helix−helix interfaces to be centered on alanine and glycine residues.

Support for a helical barrel model of HflKC oligomerization also derives from studies of the assembly and structure of the related mitochondrial prohibitin complexes by Tatsuta and co-workers (*35*). Single-particle electron microscopic studies showed purified prohibitins to form ring-shaped structures with maximal dimensions of 20−27 nm, and a circular arrangement of alternating Phb1 and Phb2 subunits was proposed. These workers suggested variability in the subunit stoichiometry and estimated that the prohibitin complex might contain 16−20 copies of each subunit, in view of the molecular weight estimated to be 1.0−1.2 million by blue native PAGE and size-exclusion chromatography (*15*, *16*). It is notable, however, that the native molecular weight has yet to be assessed by techniques that are unaffected by the protein shape, and a ring-like structure could easily result in erroneously large values by the techniques that have been used.

Tatsuta and co-workers (*35*) also identified coiled-coil sequences in the C-terminal regions of both constituent polypeptides, Phb1 and Phb2, and showed that deletion of

these regions disrupted the assembly of the prohibitin complex, even when the membrane-spanning domains were intact, implying their role in oligomerization. Furthermore, Back and co-workers (*36*) have shown that Lys-204 of Phb1 and Lys-233 of Phb2, which fall within the coiled-coil regions, can be chemically cross-linked, indicating their proximity. The Phb1 and Phb2 coiled-coil sequences are related to those that we have identified in their high frequency of positions with small conserved residues, but the pattern of these residues is not so regular as that seen for HflK and HflC in Figure 1.

Our results support a role of the coiled-coil domains of HflKC in oligomerization, but it appears that the transmembrane domains also stabilize the HflKC complex. The melting temperature of the soluble HflKC complex was low, with the T_m value being 29 °C for the most concentrated samples, and it would be expected that the membrane domains in the wild-type HflKC would provide more stability to the complex by tethering the polypeptides to the lipid bilayer and, most likely, through direct interactions as well. There are also 80 amino acid residues near the N terminus of HflK on the cytoplasmic side of the membrane that might contribute to subunit interactions. Recent evidence shows that some fraction of cellular HflKC is stably complexed with the FtsH protease in a form that sediments faster than 30S (*14*), but the excess HflKC appears to be stable without the benefit of further interactions (*6*).

While it is well-established that HflKC modulates the activity of the FtsH protease (*4*, *6*, *7*), there is little evidence of what it is that HflKC senses. Given the periplasmic location, the helical barrel structure that we propose suggests that the complex may sense some component in the environment or some condition in the periplasm.

ACKNOWLEDGMENT

The authors thank Dr. Koreaki Ito of Kyoto University for providing plasmid pKH178, Yumin Bi for expert technical assistance, and Daniel Cipriano and Paul Del Rizzo for helpful discussions and advice.

REFERENCES

1. Zorick, T. S., and Echols, H. (1991) Membrane localization of the HflA regulatory protease of *Escherichia coli* by immunoelectron microscopy, *J. Bacteriol. 173*, 6307−6310.
2. Cheng, H. H., Muhlrad, P. J., Hoyt, M. A., and Echols, H. (1988) Cleavage of the cII protein of phage λ by purified HflA protease: Control of the switch between lysis and lysogeny, *Proc. Natl. Acad. Sci. U.S.A. 85*, 7882−7886.
3. Noble, J. A., Innis, M. A., Koonin, E. V., Rudd, K. E., Banuett, F., and Herskowitz, I. (1993) The *Escherichia coli hflA* locus encodes a putative GTP-binding protein and two membrane proteins, one of which contains a protease-like domain, *Proc. Natl. Acad. Sci. U.S.A. 90*, 10866−10870.
4. Kihara, A., Akiyama, Y., and Ito, K. (1997) Host regulation of lysogenic decision in bacteriophage λ: Transmembrane modulation of FtsH (HflB), the cII degrading protease, by HflKC (HflA), *Proc. Natl. Acad. Sci. U.S.A. 94*, 5544−5549.
5. Belfort, M., and Wulff, D. L. (1971) A mutant of *Escherichia coli* that is lysogenized with high frequency, in *The Bacteriophage Lambda* (Hershey, A. D., Ed.) pp 739−742, Cold Spring Harbor Laboratory, Cold Spring Harbor, NY.
6. Kihara, A., Akiyama, Y., and Ito, K. (1996) A protease complex in the *Escherichia coli* plasma membrane: HflKC (HflA) forms a complex with FtsH (HflB), regulating its proteolytic activity against SecY, *EMBO J. 15*, 6122−6131.
7. Kihara, A., Akiyama, Y., and Ito, K. (1998) Different pathways for protein degradation by the FtsH/HflKC membrane-embedded protease complex: An implication from the interference by a mutant form of a new substrate protein, YccA, *J. Mol. Biol. 279*, 175−188.
8. Nadimpalli, R., Yalpani, N., Johal, G. S., and Simmons, C. R. (2000) Prohibitins, stomatins, and plant disease response genes compose a protein superfamily that controls cell proliferation, ion channel regulation, and death, *J. Biol. Chem. 275*, 29579−29586.
9. Langhorst, M. F., Reuter, A., and Stuermer, C. A. (2005) Scaffolding microdomains and beyond: The function of reggie/flotillin proteins, *Cell. Mol. Life Sci. 62*, 2228−2240.
10. Morrow, I. C., and Parton, R. G. (2005) Flotillins and the PHB domain protein family: Rafts, worms and anaesthetics, *Traffic 6*, 725−740.
11. Nijtmans, L. G., Artal, S. M., Grivell, L. A., and Coates, P. J. (2002) The mitochondrial PHB complex: Roles in mitochondrial respiratory complex assembly, ageing and degenerative disease, *Cell. Mol. Life Sci. 59*, 143−155.
12. Price, M. P., Thompson, R. J., Eshcol, J. O., Wemmie, J. A., and Benson, C. J. (2004) Stomatin modulates gating of acid-sensing ion channels, *J. Biol. Chem. 279*, 53886−53891.
13. Kihara, A., and Ito, K. (1998) Translocation, folding, and stability of the HflKC complex with signal anchor topogenic sequences, *J. Biol. Chem. 273*, 29770−29775.
14. Saikawa, N., Akiyama, Y., and Ito, K. (2004) FtsH exists as an exceptionally large complex containing HflKC in the plasma membrane of *Escherichia coli*, *J. Struct. Biol. 146*, 123−129.
15. Steglich, G., Neupert, W., and Langer, T. (1999) Prohibitins regulate membrane protein degradation by the m-AAA protease in mitochondria, *Mol. Cell. Biol. 19*, 3435−3442.
16. Nijtmans, L. G., de Jong, L., Artal Sanz, M., Coates, P. J., Berden, J. A., Back, J. W., Muijsers, A. O., van der Spek, H., and Grivell, L. A. (2000) Prohibitins act as a membrane-bound chaperone for the stabilization of mitochondrial proteins, *EMBO J. 19*, 2444−2451.
17. Dunn, S. D., and Chandler, J. (1998) Characterization of a *b2δ* complex from *Escherichia coli* ATP synthase, *J. Biol. Chem. 273*, 8646−8651.
18. Meselson, M., and Yuan, R. (1968) DNA restriction enzyme from *E. coli*, *Nature 217*, 1110−1114.
19. Laemmli, U. K. (1970) Cleavage of structural proteins during the assembly of the head of bacteriophage T4, *Nature 227*, 680−685.
20. Santoro, M. M., and Bolen, D. W. (1988) Unfolding free energy changes determined by the linear extrapolation method. 1. Unfolding of phenylmethanesulfonyl α-chymotrypsin using different denaturants, *Biochemistry 27*, 8063−8068.
21. Swint, L., and Robertson, A. D. (1993) Thermodynamics of unfolding for turkey ovomucoid third domain: Thermal and chemical denaturation, *Protein Sci. 2*, 2037−2049.
22. Motulsky, H., and Christopoulos, A. (2004) *Fitting Models to Biological Data Using Linear and Nonlinear Regression: A Practical Guide to Curve Fitting*, Oxford University Press, New York.
23. Cohn, E. J., and Edsall, J. T. (1943) in *Proteins, Amino Acids and Peptides*, pp 157−161, Reinhold, New York.
24. Gruber, M., Soding, J., and Lupas, A. N. (2005) REPPER—Repeats and their periodicities in fibrous proteins, *Nucleic Acids Res. 33*, W239−W243.
25. Lupas, A. (1996) Coiled coils: New structures and new functions, *Trends Biochem. Sci. 21*, 375−382.
26. Gruber, M., and Lupas, A. N. (2003) Historical review: Another 50th anniversary—New periodicities in coiled coils, *Trends Biochem. Sci. 28*, 679−685.
27. Lupas, A. N., and Gruber, M. (2005) The structure of α-helical coiled coils, *Adv. Protein Chem. 70*, 37−78.
28. Stetefeld, J., Jenny, M., Schulthess, T., Landwehr, R., Engel, J., and Kammerer, R. A. (2000) Crystal structure of a naturally occurring parallel right-handed coiled coil tetramer, *Nat. Struct. Biol. 7*, 772−776.
29. Sreerama, N., and Woody, R. W. (1993) A self-consistent method for the analysis of protein secondary structure from circular dichroism, *Anal. Biochem. 209*, 32−44.
30. Lavigne, P., Kondejewski, L. H., Houston, M. E., Jr., Sonnichsen, F. D., Lix, B., Skyes, B. D., Hodges, R. S., and Kay, C. M. (1995) Preferential heterodimeric parallel coiled-coil formation by synthetic Max and c-Myc leucine zippers: A description of putative

electrostatic interactions responsible for the specificity of heterodimerization, *J. Mol. Biol. 254*, 505−520.
31. Del Rizzo, P. A., Bi, Y., Dunn, S. D., and Shilton, B. H. (2002) The "second stalk" of *Escherichia coli* ATP synthase: Structure of the isolated dimerization domain, *Biochemistry 41*, 6875−6884.
32. Dunn, S. D., Cipriano, D. J., and Del Rizzo, P. A. (2004) ATP synthase stalk subunits *b*, *δ*, and *ϵ*: Structures and functions in energy coupling, in *Handbook of ATPases* (Futai, M., and Wada, Y., Eds.) pp 311−338, Springer-Verlag, Weinheim, Germany.
33. Koronakis, V., Sharff, A., Koronakis, E., Luisi, B., and Hughes, C. (2000) Crystal structure of the bacterial membrane protein TolC central to multidrug efflux and protein export, *Nature 405*, 914−919.
34. Bass, R. B., Strop, P., Barclay, M., and Rees, D. C. (2002) Crystal structure of *Escherichia coli* MscS, a voltage-modulated and mechanosensitive channel, *Science 298*, 1582−1587.
35. Tatsuta, T., Model, K., and Langer, T. (2005) Formation of membrane-bound ring complexes by prohibitins in mitochondria, *Mol. Biol. Cell 16*, 248−259.
36. Back, J. W., Sanz, M. A., de Jong, L., de Koning, L. J., Nijtmans, L. G., de Koster, C. G., Grivell, L. A., van der Spek, H., and Muijsers, A. O. (2002) A structure for the yeast prohibitin complex: Structure prediction and evidence from chemical crosslinking and mass spectrometry, *Protein Sci. 11*, 2471−2478.

BI0606997